PERGAMON

Atmospheric Environment 33 (1999) 3897–3909

ATMOSPHERIC ENVIRONMENT

Impact of anthropogenic heat on urban climate in Tokyo

Toshiaki Ichinose[a,*], Kazuhiro Shimodozono[b], Keisuke Hanaki[b]

[a]*Center for Global Environmental Research, National Institute for Environmental Studies, 16-2, Onogawa, Tsukuba 305-0053, Japan*
[b]*Research Center for Advanced Science and Technology, The University of Tokyo, 4-6-1, Komaba, Meguro-ku, Tokyo 153, Japan*

Abstract

This study quantifies the contribution through energy consumption, to the heat island phenomena and discussed how reductions in energy consumption could mitigate impacts on the urban thermal environment. Very detailed maps of anthropogenic heat in Tokyo were drawn with data from energy statistics and a very detailed digital geographic land use data set including the number of stories of building at each grid point. Animated computer graphics of the annual and diurnal variability in Tokyo's anthropogenic heat were also prepared with the same data sources. These outputs characterize scenarios of anthropogenic heat emission and can be applied to a numerical simulation model of the local climate. The anthropogenic heat flux in central Tokyo exceeded 400 W m^{-2} in daytime, and the maximum value was 1590 W m^{-2} in winter. The hot water supply in offices and hotels contributed 51% of this 1590 W m^{-2}. The anthropogenic heat flux from the household sector in the suburbs reached about 30 W m^{-2} at night. Numerical simulations of urban climate in Tokyo were performed by referring to these maps. A heat island appeared evident in winter because of weakness of the sea breeze from Tokyo Bay. At 8 p.m., several peaks of high-temperature appeared, around Otemachi, Shinjuku and Ikebukuro; the areas with the largest anthropogenic heat fluxes. In summer the shortwave radiation was strong and the influence of anthropogenic heat was relatively small. In winter, on the other hand, the shortwave radiation was weak and the influence of anthropogenic heat was relatively large. The effects of reducing energy consumption, by 50% for hot water supply and 100% for space cooling, on near surface air temperature would be at most -0.5°C.

Keywords: Anthropogenic heat; Urban area; Digital geographic data; Tokyo; Numerical simulation

1. Introduction

Expansion of urban areas and increases in urban activity have several impacts on urban environments. These impacts are represented by air pollution, water pollution, thermal pollution, caused by anthropogenic heat emission, and so on. It is theoretically impossible to eliminate anthropogenic heat from energy consumption just as it is impractical to completely eliminate air or water pollution. Anthropogenic heat affects local climate in urban areas producing phenomena such as heat islands. This process has been explored in a numerical simulation (Kimura and Takahashi, 1991). Recently, it was reported that urbanization has both positive and negetive impacts on thermal environment, as an increase in urban energy use and a decrease in incoming solar radiation (Stanhill and Kalma, 1995).

On the other hand, evaluation of the impact of urban activity through land use change and anthropogenic heat on the urban thermal environment has been required in view of urban planning. Quantitative analysis of how urban structures and human activities should be changed to reduce heat island phenomena requires detailed data on anthropogenic heat sources, one of the surface boundary conditions, for use in numerical simulations of such impacts. Such analysis needs evaluation of the influence of temporal and spatial structures of anthropogenic heat on urban thermal environment.

There have been many large-scale analyses of urban energy consumption as a source of anthropogenic heat (e.g. Ichinose et al., 1993). However, the temporal and spatial variability in urban areas have not been adequately studied. One apparent reason for this deficiency

* Corresponding author.

1352-2310/99/$ - see front matter
PII: S1352-2310(99)00132-6

is that field surveys of energy consumption over wide areas are difficult to carry out. The data for energy consumption as a source of anthropogenic heat, as one of the surface boundary conditions for numerical simulations of local climate, must be in the form of mesh data to be referenced geographically. Some studies which mapped the anthropogenic heat in Tokyo have been published (Kimura and Takahashi, 1991; Narita and Maekawa, 1991; Saitoh et al., 1992), but they do not present the detailed procedures used to estimate the value at each mesh point. Few studies mention annual and diurnal variability.

A time-series analysis of the distribution of urban energy consumption is, therefore, necessary to evaluate its impact on the thermal environment. In this study, a detailed analysis of the temporal variability of the distribution of energy consumption in the 23 special wards of the Tokyo Metropolis (Tokyo) was attempted. The authors used a digital geographic land use data set containing the number of stories of building at each grid point to tabulate energy consumption on an areal basis. The numerical simulation of local climate was consequently performed to determine the effect of anthropogenic heat on Tokyo's urban climate. Generally, the arrangement of such data set has never been adequately promoted. To treat the temporal and spatial variability in the numerical simulation of local climate is not difficult. But such delay in data arrangement has made it difficult. This study is the first attempt to treat the temporal and spatial structures using such data set which has been arranged recently.

2. Time-series variability of the distribution of urban anthropogenic heat in Tokyo

2.1. Estimation of areal energy consumption in Tokyo

Hiramatsu et al. (1992) estimated the amount of energy consumption in Tokyo in 1989 in each sector (household, commercial, manufacturing and transportation) and for each kind of fuel (Fig. 1) with data from energy statistics. These amounts must be divided into purposes (space cooling, space heating, hot water supply, kitchen and utilities; in the cases of the household and commercial sectors) to express annual and diurnal variability in energy consumption.

The commercial sector comprises several kinds of businesses. The intensity of energy use and fuel mix vary by business. Ichinose et al. (1994) determined areal energy consumption in Tokyo in 1989 by business, from several kinds of energy statistics and a digital geographic land use data set containing the number of stories of building at each grid point (Fig. 2). They determined and showed areal energy consumption in other three sectors. In the cases of the manufacturing and transportation sectors,

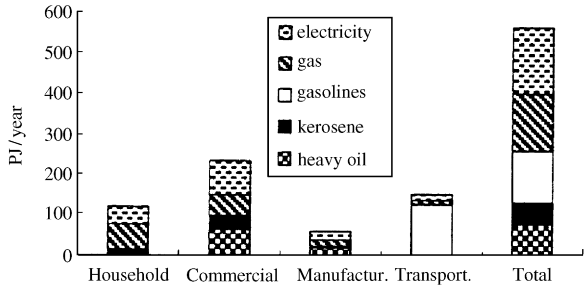

Fig. 1. Energy consumption in Tokyo in 1989. Revised from Hiramatsu et al. (1992) by Ichinose et al. (1994). "Gas" consists of city gas (76%) and LPG (24%). "Gasolines" consist of gasoline (61%) and light oil (39%).

the amount of areal energy consumption was not divided into purposes. The above-mentioned data set was created by the Bureau of Urban Planning of the Tokyo Metropolitan Government. In this data set, the interval between grid points is 25 m and the dominant kind of business (including residence or apartment house) and number of stories of each building present on each grid point were recorded. For grid points with no buildings, land use was recorded. More than 17 categories on business or land use regarded as anthropogenic heat source were cataloged in this data set. Ichinose et al. (1994) arranged them into 12 categories (office, education, welfare, department store, shop, hotel, leisure, residence, apartment house, industry, vehicle and train) shown in Fig. 2. When each grid point above mentioned was regarded as the square of 625 m^2, the integrated amount of areal energy consumption in Fig. 2 with the square of floor was same with the result shown in Fig. 1.

Fig. 2 showed that large amounts of energy were consumed by welfare (hospitals and health care facilities) and hotels due to high demand for hot water. High demand for space heating in welfare and leisure (amusement places) and for appliances (utilities) in department stores and leisure were also found.

2.2. Annual and diurnal variability of energy consumption

Ichinose et al. (1994) divided annual values (see Fig. 2) by season and by hour, and analyzed the patterns of annual and diurnal variability associated with each purpose for each category of business or land use. Most of their patterns were determined referring to a survey by the Bureau of Environmental Preservation of the Tokyo Metropolitan Government (Pers. Comm.). It showed many patterns of annual and diurnal variability associated with each purpose for each category of business.

In summer, the demand for space cooling during daytime was fairly constant (Fig. 3). Nighttime demand from hotels was not insignificant. A small peak in residential demand was detected at around 9 p.m.

Fig. 2. Areal energy consumption for each category on business or land use in Tokyo in 1989, excluding 2.179 GJ m^{-2} yr^{-1} for industry, 1.393 GJ m^{-2} yr^{-1} for motor vehicles and 0.918 GJ m^{-2} yr^{-1} for trains. "Depart. s." means department store. "Apart. h." means apartment house. Taken from Ichinose et al. (1994).

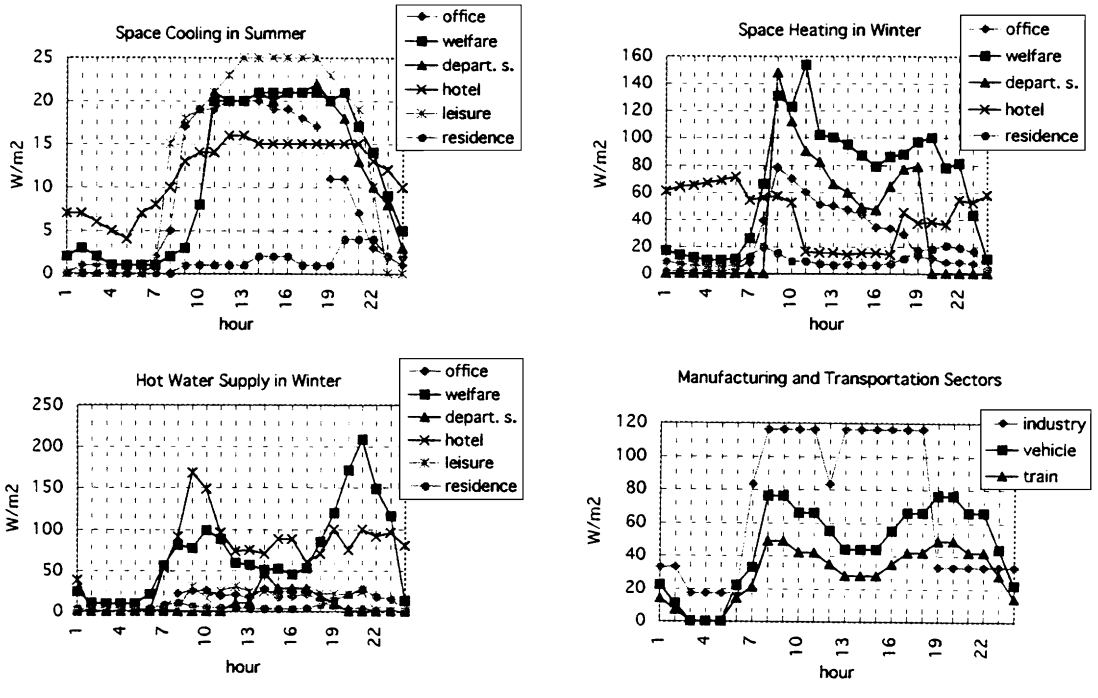

Fig. 3. Diurnal variability of demand for space cooling in summer, space heating in winter and hot water supply in winter. "Depart. s." means department store. Additionally diurnal variability of areal energy consumption in the manufacturing and transportation sectors are also shown. Taken from Ichinose et al. (1994).

In winter, office demand for space heating peaked at around 9 a.m., and decreased slowly through daytime. Hotels had low demand from check-out time until check-in time and a large demand at night. Residential demand had twin peaks at 8 a.m. and 9 p.m. For hot water, a morning peak in hotels demand and an evening peak in welfare demand were noteworthy.

Only diurnal variability was analyzed for the manufacturing (industry) and transportation (motor vehicle and train) sectors. These patterns were applied to all seasons.

2.3. Computer mapping of urban anthropogenic heat

In this study, energy consumption is assumed to be equivalent to anthropogenic heat, since ultimately, all consumed energy is transformed into heat. However, the delay of heat transfer from appliances or buildings to the

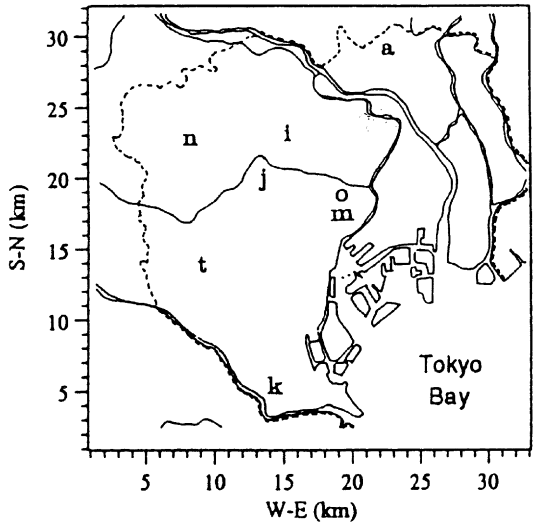

Fig. 4. Study area and main stations for measurement of near surface air temperature. Dotted line means the margin of the 23 special wards of the Tokyo Metropolis. Symbols as follows: n: Nakano, t: Setagaya, j: Shinjuku, i: Ikebukuro, k: Kamata, m: Marunouchi, o: Otemachi, a: Adachi. All of stations shown here, except Otemachi (AMeDAS; Automated Meteorological Data Acquisition System, operated by the Japan Meteorological Agency), are operated by the Tokyo Metropolitan Government.

atmosphere is neglected by this assumption. A not insignificant part of the energy consumed for hot water supply enters sewers. Heat from appliances, especially that from space cooling appliances, consists of sensible heat and latent heat. These components must be individually considered. In this study, all of anthropogenic heat is regarded as sensible heat to consider the case where the thermal impact on urban atmosphere is strongest.

Since energy consumption in the transportation sector is not proportional to area, mapping of this sector's areal energy consumption is difficult because of the lack of adequate data. This study allocated this value on the grid point where road or railway was present. Namely, the authors assumed that traffic density was spatially uniform.

The anthropogenic heat in the 23 wards of Tokyo (see Fig. 4) was mapped on a computer with the digital geographic land use data set previously mentioned and the areal energy consumption data (Ichinose et al., 1994). The diurnal changes in the spatial distribution of anthropogenic heat in Tokyo were visualized with computer graphics animation. The spatial resolution of the images was 250 m. The snapshots of this animation are shown in Fig. 5. The central business district (CBD) contained a large amount of anthropogenic heat at 2 p.m. during winter. High-density areas such as Marunouchi, Shinjuku, Shibuya and Ikebukuro or huge green spaces such as the imperial palace grounds, Yoyogi Park and the Ara

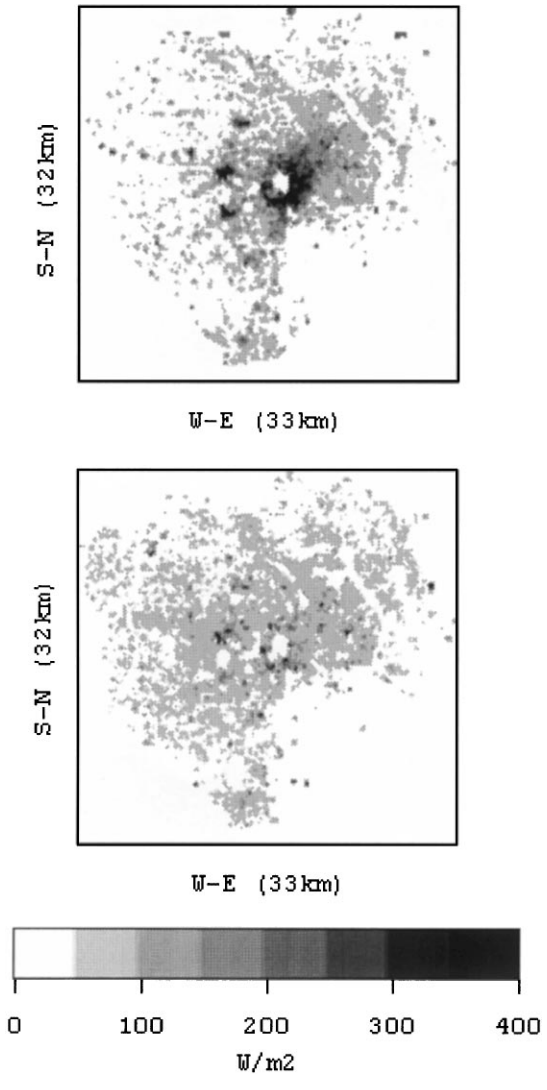

Fig. 5. Distribution of anthropogenic heat in Tokyo at 2 p.m. (upper) and 9 p.m. (lower) in winter. Range indicated in the color bar runs from zero (white) to 400 W m^{-2} (black).

River could be clearly distinguished. However, the residential area around the CBD contained more anthropogenic heat at 9 p.m. than at 2 p.m., and the contrast with the CBD became small.

According to Saitoh et al. (1992), the amount of energy consumption in Otemachi at central Tokyo exceeds 120 W m^{-2} in summer. This value represents a grid cell of 1 km width. In the authors' study, 1590 W m^{-2} was released from a unit mesh in Shinjuku at 9 a.m. in winter as the maximum value. The contribution of space heating was 34% of this total and that of hot water supply was 51%. This mesh contained two office buildings of 48 stories and a hotel of 47 stories, which contributed 31 and 67% of the total, respectively. In summer the same mesh

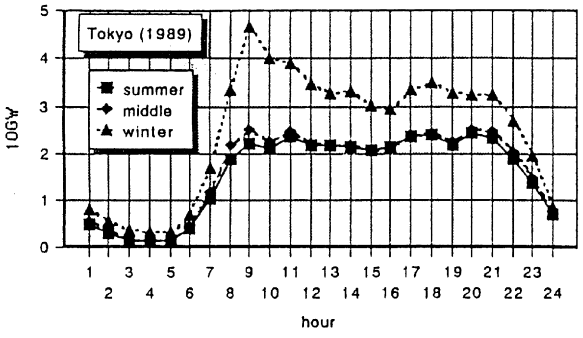

Fig. 6. Diurnal variability of gross anthropogenic heat in Tokyo in each season. "Middle" means spring and autumn.

released a maximum of 908 W m^{-2} at 9 a.m. and the share of this total contributed by space cooling was 13%. Areas releasing more than 400 W m^{-2} were found around Marunouchi and Shinjuku at 2 p.m., while at 9 p.m. the residential area with relative great value showed around 30 W m^{-2} and the areas under 100 W m^{-2} became evident even in the CBD. Gross anthropogenic heat in Tokyo peaked at 9 a.m. in winter and then was essentially constant until 9 p.m. except in winter (Fig. 6). Clearly, in these seasons, the center of energy consumption could be regarded as moving from the city to the suburbs with the movement of people.

This study neglected the contributions of human metabolic energy, incineration plants and power plants, because of difficulties in mapping them. In the digital geographic land use data set the authors used, they were not identified. The contribution of human metabolic energy in Tokyo has been estimated to be around 5–10% of the total (Morita, 1993). According to a survey (1991–1993) by the Technical Research Institute, Obayashi Corporation (Pers. Comm.), there are the following heat sources in the 23 wards of Tokyo. Two power plants, 12 sewage incineration plants and 14 garbage incineration plants were estimated to release 32.6, 13.8 and 19.0 PJ yr^{-1}, respectively. These total reaches around 11% of the total amount shown in Fig. 1.

3. Numerical simulation of urban climate

3.1. Numerical simulation model for local climate

The numerical simulation model used in this study was based on the Colorado State University Mesoscale Model (CSU-MM) (Pielke, 1974) with the modifications of Ulrickson and Mass (1990) and Kessler and Douglas (1992) and with small changes to input values for several surface boundary conditions like albedo or anthropogenic heat in each grid cell. Hydrostatic equilibrium and the Boussinesq approximation are assumed in this model. The model consists of equations of motion, moisture and continuity within a three-dimensional terrain-following coordinate system and it includes a thermodynamic equation, a diagnostic equation for pressure and an equation for surface heat budget. Exchange coefficients are computed from turbulent kinetic energy and turbulent length scale due to Therry and Lacarrere (1983). Planetary boundary layer depth is given with the methodology of Ulrickson and Mass (1990). Energy balance at the surface, including a term for anthropogenic heat, is expressed as

$$Q = S + I - H - L - C - G + A, \quad (1)$$

where Q is the heat stored in the surface layer of the soil, S is the net shortwave radiation flux at the ground surface, I is the incoming infrared radiation from the atmosphere, H is the sensible heat flux, L is the latent heat flux, C is the outgoing infrared radiation from the surface, G is the heat conducted into the soil layer and A is anthropogenic heat flux. I is calculated considering the influence of only carbon dioxide and moisture. The potential temperature in the soil layer is calculated with a heat conductivity equation.

A rectangular area fitting the 23 wards of Tokyo was divided by a grid system with 33 grid cells on the east–west axis and 32 on the north–south axis (see Fig. 4). Each horizontal grid was 1000 m on each side. The atmosphere (up to 8000 m) was divided into 23 layers of different thickness, from a minimum of 5 m near the surface to a maximum of 1000 m at the top of this domain. The soil to a depth of 0.5 m is also divided into 11 layers of varying thickness. The surface boundary conditions in each grid cell, i.e., albedo, evaporation efficiency, roughness length, density, specific heat capacity, heat diffusion coefficient, were calculated by the method of a weighted average for each square of land use using the digital geographic land use data set previously mentioned. The surface parameters for each land use were determined (Table 1) referring to Anthes et al. (1987). It was difficult to use the classification of categories on business or land use cataloged on that data set directly. The classification of land use was, therefore, newly determined. Since such a data set contains information about the number of stories of building at each grid point, anthropogenic heat can be found for every height. However, in this study, all anthropogenic heat was released on the ground surface, while the urban canopy layer has been omitted from the model.

The time step for numerical integration was chosen as 10 s and results were calculated for 24 h from 6 a.m. on each studied date. Typical weather conditions under which the impact of anthropogenic heat on urban climate is significant are cloudless and calm. Four such summer days (21, 22 and 23 July and 8 August 1989) and three such winter days (2, 3 and 4 February 1989) were selected

Table 1
Surface parameters for each land use (based on Anthes et al., 1987)

Land Use	Albedo	Evaporation efficiency	Roughness length (m)	Density (kg m^{-3})	Specific heat capacity (J kg^{-1} K^{-1})	Heat diffusion coefficient (10^{-7} m^2 s^{-1})
Rice paddy	0.17	0.50	0.1	1800	1173	5.3
Vegetable field	0.17	0.30	0.1	1800	1173	5.3
Orchard	0.16	0.30	0.5	1800	1173	5.3
Lawn and park	0.16	0.30	0.5	1800	1173	5.3
Forest	0.16	0.35	0.5	1800	1173	5.3
Yard	0.14	0.20	0.15	1800	1173	5.3
Built-up area	0.18	0.05	0.5	2400	880	7.2
Traffic use	0.18	0.05	0.5	2100	880	3.8
Other use	0.18	0.10	0.2	1800	1173	5.3
Surface water	0.08	1.00	10^{-7}	1000	4190	5.3

"Traffic Use" consists of motorway and railway.

Table 2
Initial conditions for numerical simulations (values at 6 a.m.)

	Summer	Winter
Date	July 22	February 3
Surface air pressure (hPa)	1000	1010
Soil and surface air Temperature (K)	298.0	276.0
Sea surface temperature (K)	298.0	280.0
Vertical gradient of potential Temperature (K m^{-1})	0.0055	0.0060
Surface relative humidity (%)	70.0	60.0
Wind direction	S	NW
Wind velocity (m s^{-1})	0.5	0.5

Initial wind direction and velocity are assumed to be constant in all of layers of the atmosphere.

based on synoptic weather observations around Japan and the meteorological data from the AMeDAS weather stations (Automated Meteorological Data Acquisition System, operated by the Japan Meteorological Agency) around Tokyo. The initial conditions over the land portion of the whole study area, such as near surface air temperature, relative humidity and wind direction and velocity, at 6 a.m. were assumed to be constant and equivalent to the average values of all sample dates observed at the Otemachi AMeDAS station (Table 2). The elevation of the ground surface was assumed to be zero for the whole area. Since this area is almost flat, this approximation appears reasonable when compared with the average elevation for each grid cell. Additionally, lateral boundary conditions were assumed to be of zero gradient.

3.2. Result of numerical simulation

The authors assumed that the second layer was centred 7.5 m above the ground and modeled the horizontal distributions of air temperature and wind at that elevation in summer (Fig. 7) and in winter (Fig. 8).

The difference between near surface air temperatures above land and sea reached about 5°C and a sea breeze at near surface level developed to about 5 m s^{-1} at 11 a.m. in summer. In the areas affected by the sea breeze, the isothermal lines were nearly parallel with the sea shore and the intervals between them were nearly constant. These features are a result of air mass modification by the differences in heat fluxes between sea and land (Stull, 1994). Along the shore, the isothermal lines were complicated because of small patches of reclaimed land. By 2 p.m., the sea breeze penetrated far into shore, dissipating the relatively high temperatures which had been present at 11 a.m. By 8 p.m., the horizontal gradient of near surface air temperature had become small due to cooling on land, in contrast to the large gradient observed during daytime. By 11 p.m. it was nearly calm on land and a local heat island around Shinjuku and a cliff along the Ara River had appeared.

In winter, the heat island at 11 a.m. was more distinct than in summer. The core of the heat island was around Marunouchi and a steep temperature gradient formed at the side of Tokyo Bay. By 2 p.m., the difference between near surface air temperatures above land and sea had reached about 4°C and a sea breeze had penetrated around Shinjuku with a velocity of about 3–4 m s^{-1}. The core of the heat island had moved to Shinjuku; the downwind side of Marunouchi. By 5 p.m., the sea breeze had reached Setagaya, Nakano and Adachi. The pattern of isothermal lines was similar to that in summer, but the intervals between isothermal lines around Otemachi and Shinjuku were wide because of anthropogenic heat release. By 8 p.m., the sea breeze had weakened with rapid cooling on land and a heat island again appeared; high temperature peaks appeared around Otemachi, Shinjuku and Ikebukuro, the areas with the greatest

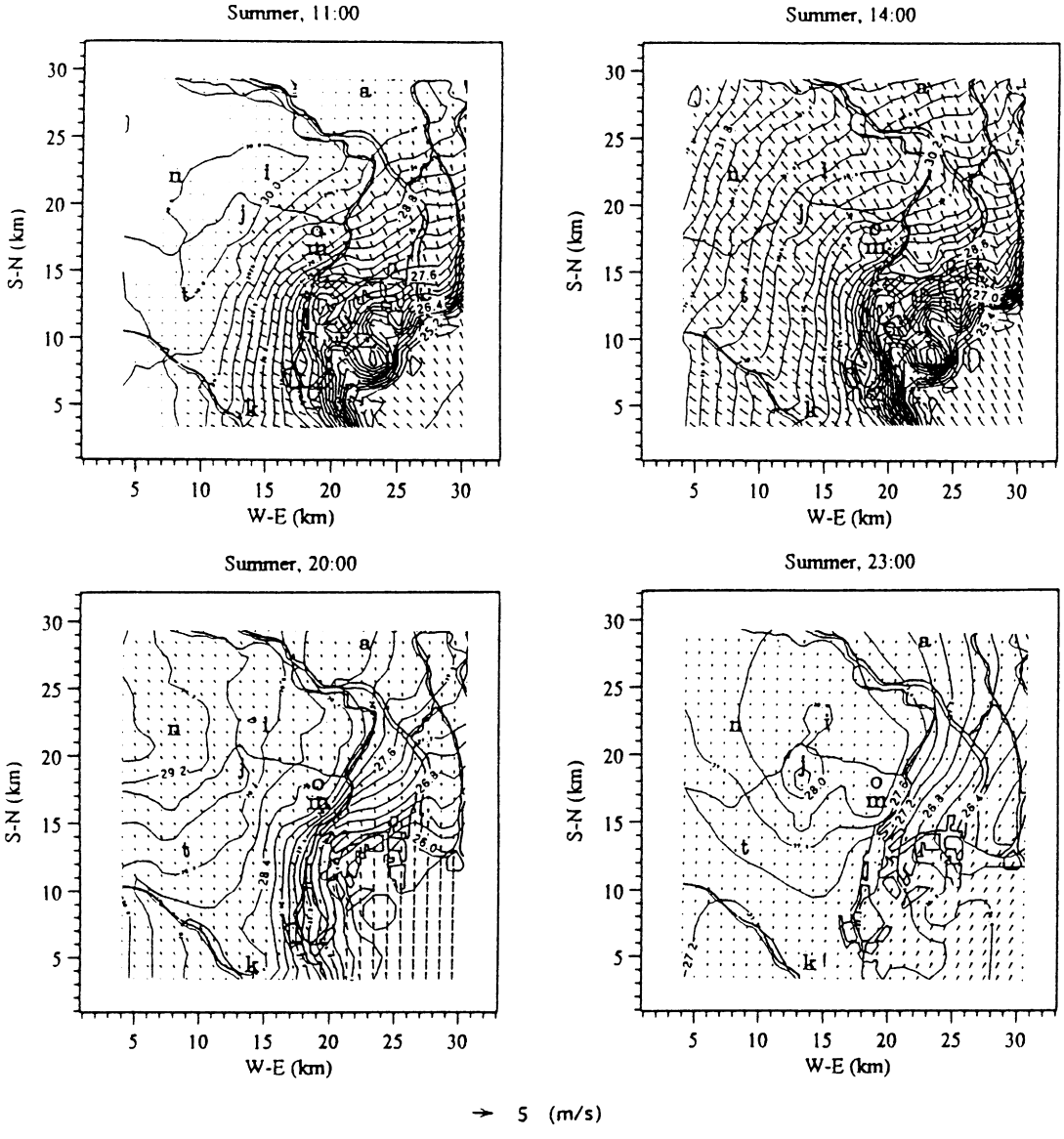

Fig. 7. Horizontal distributions of air temperatures (°C) and wind system at 7.5 m above the ground in summer. Symbols as in Fig. 4.

anthropogenic heat fluxes. A heat island also formed around Kamata, in the southern part of Tokyo. In winter, these heat islands persisted beyond midnight. The core of the heat island around Otemachi appearing in winter did not occur in summer because of the sea breeze.

3.3. Surface heat budget

The authors evaluated the heat budget in central Tokyo (in the grid cell including Otemachi; typical highly built-up area in central Tokyo) for each season (Fig. 9). In Fig. 9, net infrared radiation is dealt with as longwave radiation. Shortwave radiation was dominant during daytime in summer, reaching a maximum of more than 800 W m^{-2} at noon. In contrast, anthropogenic heat was only about a fourth of that amount. Anthropogenic heat release was constant at around 200 W m^{-2} during daytime and decreased gradually after sunset. In the morning, heat conduction into the soil layer was relatively large, rising until it peaked at 9 a.m. Thereafter, it decreased due to thermal saturation of the soil layer. The sensible and latent heat fluxes reached a maximum at 1 p.m., whereas the shortwave radiation peaked at noon. The maximum sensible heat flux was around 300 W m^{-2}.

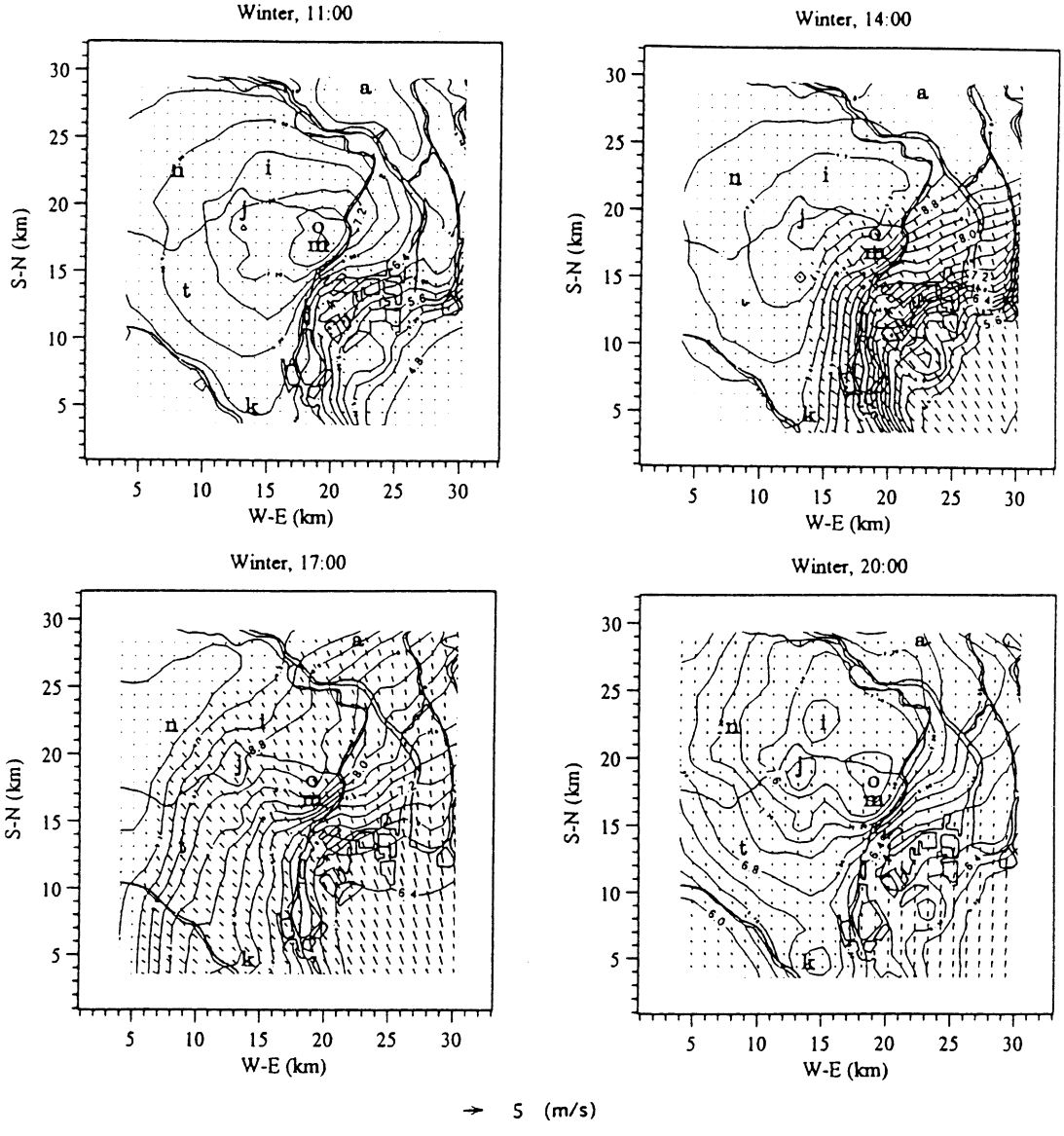

Fig. 8. As in Fig. 7, but in winter. Symbols as in Fig. 4.

The latent heat flux was about 30% greater than the sensible heat flux in daytime because of the presence in this grid cell of the large moat around the imperial palace. After sunset (7 p.m.) the sensible and latent heat fluxes soon reached around zero. The direction of heat conduction in the soil layer reversed at 5 p.m. and it balanced the net longwave radiation.

Maximum shortwave radiation in winter was around 550 W m^{-2}, around 40% less than that in summer. In contrast to summer, the anthropogenic heat at 8 a.m. reached a maximum twice that of summer and nearly equivalent to the shortwave radiation. Heat conduction into the soil layer increased rapidly after 7 a.m. (sunrise) and peaked at around 400 W m^{-2} at 11 a.m., greater than the 300 W m^{-2} in summer. The sensible heat flux had two peaks at 10 a.m. and 1 p.m., corresponding to peaks in the anthropogenic heat and the shortwave radiation flux, respectively. The latent heat flux was around half of the sensible heat flux. The maximum of the net longwave radiation and the reverse direction heat conduction in the soil layer came 1 h earlier than those in summer. At night, the net longwave radiation, anthropogenic heat and heat conduction in the soil layer balanced one another.

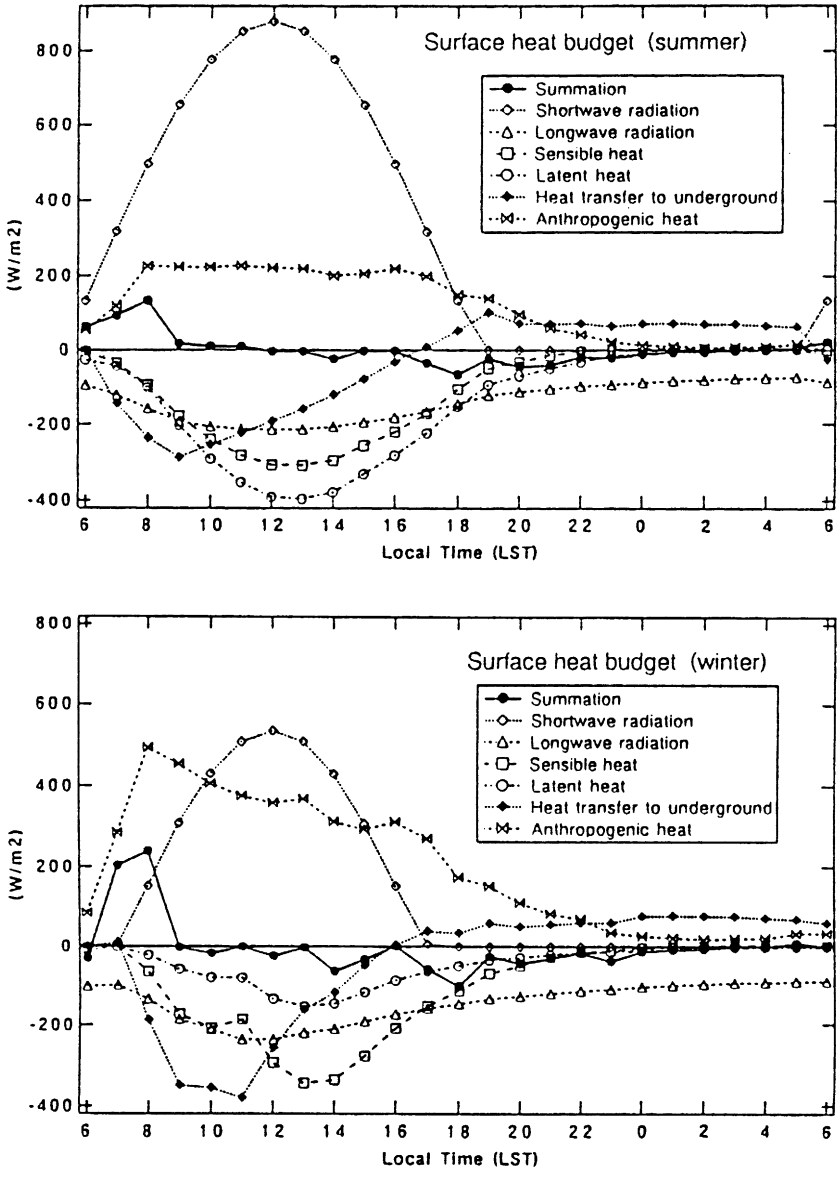

Fig. 9. Surface heat budget in central Tokyo (in the grid cell including Otemachi). Net infrared radiation is dealt with here as longwave radiation. Positive values indicate heat flux into the ground surface. Thus sensible heat flux from the ground surface and heat conduction into the soil layer are expressed as negative values. Symbols listed in legend correspond to each term on Eq. (1); $Q, S, I–C, –H, –L, –G, A$, from above, respectively.

3.4. Validation of results

The validity of the results of this numerical simulation was evaluated by comparing the simulated air temperatures at the height of 7.5 m above the ground and the observed values (average of all sample dates). The data from three AMeDAS stations (Otemachi, Nakaarai and Shinkiba) and 22 Tokyo Metropolitan Government stations (hourly atmospheric environment data) were used as the observed values (refer also Fig. 4). The latter data set has sufficient spatial density to represent the horizontal distribution of near surface air temperatures on the scale of Tokyo, but the reliability of the data is not high, because the conditions at some observatories are inadequate for observations of parameters such as near surface air temperature, for various reasons; e.g. the observatory on the roof top of a building.

In summer, the simulated near surface air temperatures for 17 points around the center of the study area, for instance, Otemachi (Fig. 10), showed close values to

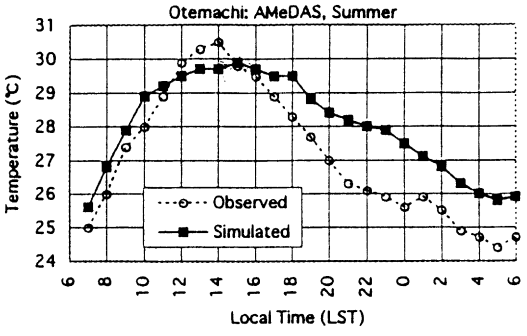

Fig. 10. Diurnal variability of observed and simulated near surface air temperatures in summer at Otemachi.

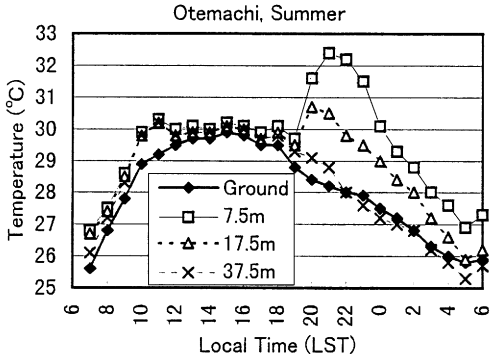

Fig. 11. Comparison of diurnal variability of simulated near surface air temperatures between the different heights at which anthropogenic heat was given. Anthropogenic heat was introduced into the ground surface as the heat flux in the case of 'Ground'. In the cases of 7.5, 17.5 and 37.5 m, anthropogenic heat was emitted directly to atmosphere at the second, the third and the fourth layer, respectively. These heights mean the center of each layer.

the observed data for daytime, but the simulated temperatures from evening to early morning tended to be 2–3°C higher than those actually measured. The authors regard a delay in the influence of anthropogenic heat to the near surface air temperature and their failure to consider the emission height of anthropogenic heat as reasons for these discrepancies. Such discrepancies are inevitable when treating all of the anthropogenic heat, including that from middle and high stories, as emerging near the ground surface. The urban canopy is also not expressed in this model. Though the reliability of the results depends on the accuracy of the simulated wind system, the domain in this simulation is fairly narrow to express the effects of the mesoscale circulation between the high central mountainous area of Japan and the Pacific Ocean (Kondo, 1990).

The methodology of introducing anthropogenic heat into the surface layer as the heat flux will also cause serious effects on the ground surface temperature and on sensible heat flux at the ground surface, because some part of anthropogenic heat is apparently to be emitted directly to atmosphere, whereas some other part is stored in the wall of buildings. However a detailed behavior of anthropogenic heat has never been adequately studied. The authors attempted, therefore, an examination of this problem (Fig. 11). Anthropogenic heat was introduced into the ground surface as the heat flux in the case of 'Ground'. This is the same curve 'Simulated' in Fig. 10. In the cases of 7.5, 17.5 and 37.5 m, anthropogenic heat was emitted directly to atmosphere at the second, the third and the fourth layer, respectively. The latter cases showed the diurnal variabilities which were greatly apart from an observed variability (see Fig. 10). Extraordinarily high temperatures were calculated because of the stabilization of the surface boundary layer at night, especially from mid-afternoon until late evening. Simulations on the detailed variabilities of the ground surface temperature and the sensible heat flux at the ground surface are also out of the aim of this study. So far as this model is used, the methodology shown in this study might be better. However a treatment of anthropogenic heat in the numerical model should be discussed in detail in the future.

4. Impact of urban structure and human activity

4.1. Contribution of anthropogenic heat and land coverage

Otemachi (in summer) and Shinjuku (in winter) were selected for analysis of the impact of anthropogenic heat on the urban thermal environment because the simulated temperatures at those points (and in those seasons) showed close values to those observed for daytime. To estimate the contributions of anthropogenic heat and land coverage to the formation of urban heat islands, temperatures simulated under various conditions were compared (Table 3).

The difference between Case 1 (present conditions) and Case 2 (without anthropogenic heat) was small during daytime in summer, but rapidly increased from mid-afternoon until late evening (Fig. 12). This difference was large for sites near large releases of anthropogenic heat; the maximum was around 1.5°C in Otemachi at 10 p.m. Though the maximum of anthropogenic heat flux occurred during daytime, its influence was more striking at night. The temperature difference between the cases with and without anthropogenic heat was smallest near dawn. On the other hand, the difference between Cases 2 and 3 (all of the study area is assumed to be a grassland) gradually increased during daytime but remained around 1°C all day. In contrast with the modest effect of anthropogenic heat, land coverage strongly affected the near surface air temperature during the heating stage. In Otemachi, the sensible and latent heat fluxes of Case 1 in

Table 3
Condition for anthropogenic heat and land coverage in each scenario

	Anthropogenic heat	Land coverage
Case 1	Included	Current situation
Case 2	Not included	Current situation
Case 3	Not included	All of the study area is assumed to be a grassland
Case 4	The reduction of 50% for hot water supply	Current situation
Case 5	The reduction of 50% for hot water supply and 100% for space cooling	Current situation

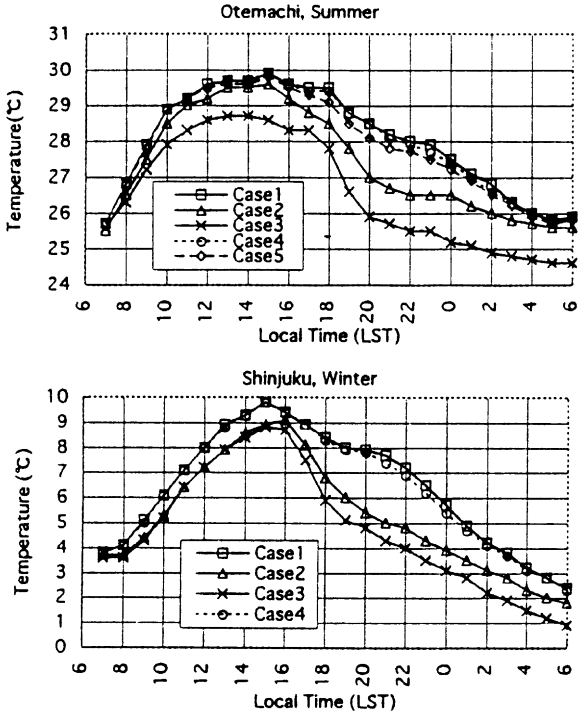

Fig. 12. Comparison of diurnal variability of simulated near surface air temperatures. Conditions of each scenario are shown in Table 3.

daytime (see Fig. 9) were greater than those of Case 2 (Fig. 13), but there was little difference in net longwave radiation. The reverse in the direction of heat conduction in the soil layer in Case 2 came around 1 h earlier than that in Case 1.

In contrast to the small effect of anthropogenic heat flux in summer, the temperature simulated in Case 1 for the whole day in winter was higher than that for Case 2. The difference was particularly large for the period from mid-afternoon until late evening, with a maximum of around 2.5°C at 9 p.m. (Fig. 12). In daytime, there was little difference between Cases 2 and 3, with the difference from evening through the night constant at around 1°C. The sensible and latent heat fluxes in Otemachi varied with variability in anthropogenic heat flux (in Case 1, see Fig. 9). In contrast, both of these fluxes were very small for Case 2 (Fig. 13). The sensible and latent heat fluxes and the net longwave radiation in Case 2 peaked around 1 h later than in Case 1. The reverse in the direction of heat conduction in the soil layer came 1 h earlier than that for Case 1. In Case 1, sensible heat flux continued at 50–100 W m^{-2} for a few hours after sunset. This continuing flux of sensible heat seemed to be one cause of the nocturnal heat island observed in winter.

As mentioned above, in summer the shortwave radiation was strong and the influence of anthropogenic heat was relatively small. In winter, on the other hand, the shortwave radiation was weak and the influence of anthropogenic heat was relatively large.

4.2. Effect of introduction of district heating systems

Actually, anthropogenic heat cannot be reduced easily; energy-saving scenarios based on specific technologies can be simulated. For example, energy consumption per unit heat demand can be reduced by introducing district heating (or cooling) systems. In case of hot water supply using gas in households and offices, the heating efficiency is low and a not insignificant amount of heat is wasted in the process of boiling. However, if hot water is supplied by district heating systems, anthropogenic heat can be reduced because most of such heat losses are averted. The authors simulated two such scenarios in which introduction of district heating (or cooling) systems could reduce 50% of the energy consumption for hot water supply (Case 4, Table 3) or 50% of the energy consumption for hot water supply and 100% of that for space cooling (Case 5, Table 3). But the decline in temperature under the latter scenario was only 0.5°C or less, the maximum at night. This result showed that it was difficult to mitigate the urban climate by merely reducing heat loss by introducing district heating (or cooling) systems (Fig. 12).

5. Conclusions

The results of this study are summarized as follows:

(1) Very detailed maps of anthropogenic heat in Tokyo were drawn using data from energy statistics and

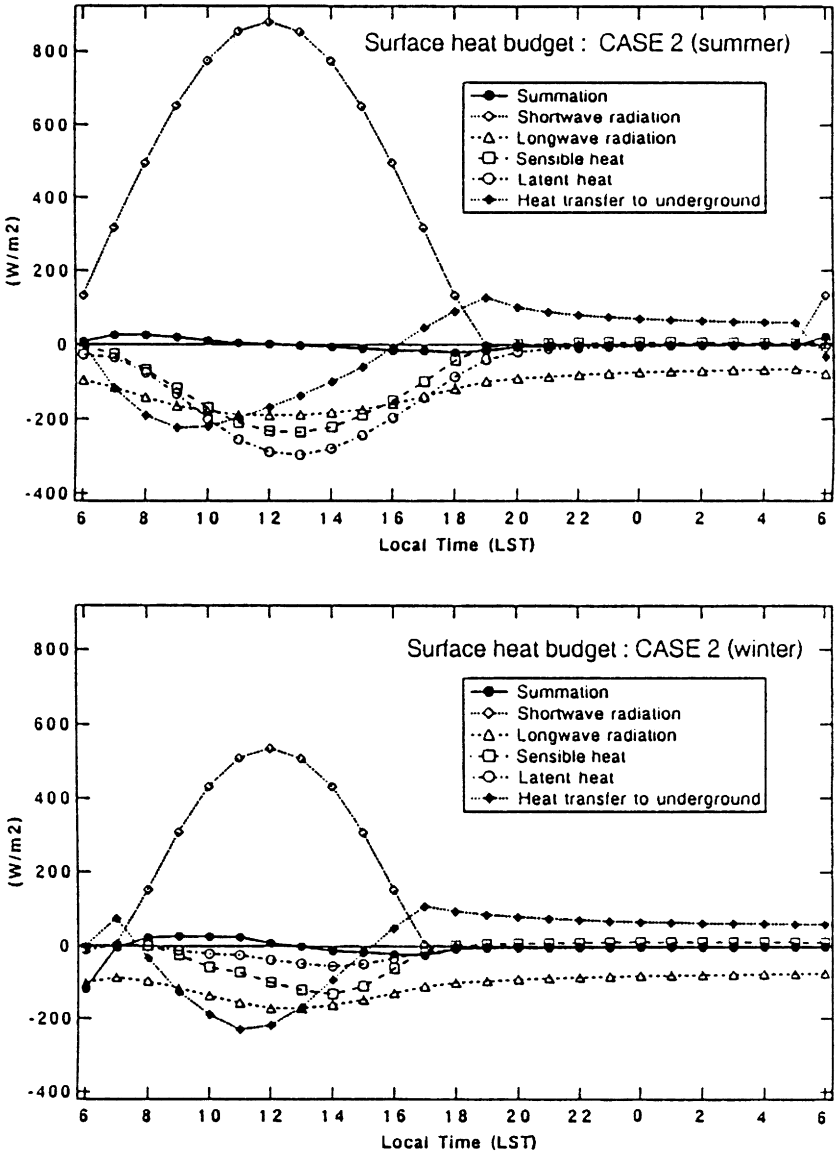

Fig. 13. As in Fig. 9, but for Case 2 (without anthropogenic heat).

a very detailed digital geographic land use data set containing the number of stories of building at each grid point. The anthropogenic heat in central Tokyo exceeded 400 W m^{-2} in daytime and the maximum value was 1590 W m^{-2} in winter.

(2) Numerical simulations of the urban climate of Tokyo were performed. In winter, heat islands seemed to occur mainly due to weakness of the sea breeze from Tokyo Bay. At 8 p.m. several peaks of high-temperature appeared, around Otemachi, Shinjuku and Ikebukuro, the areas with largest fluxes of anthropogenic heat.

(3) In summer the shortwave radiation was strong and the influence of anthropogenic heat was relatively small. In winter, on the other hand, the shortwave radiation was weak and the influence of anthropogenic heat was relatively large. The effect on near surface air temperature of reductions in energy consumption by 50% for hot water supply and by 100% for space cooling would be at most $-0.5°C$.

Acknowledgements

The authors would like to express their sincere thanks to Dr. Itsushi Uno of National Institute for Environmental Studies for advice on the modification of CSU-

MM. The authors would also like to thank the Bureau of Urban Planning and the Bureau of Sewerage, both of the Tokyo Metropolitan Government, for access to their digital geographic land use data set for Tokyo. The Bureau of Environmental Preservation of the Tokyo Metropolitan Government is acknowledged for providing hourly data on the atmospheric environment of Tokyo and the Japan Meteorological Agency for providing the hourly AMeDAS data for Tokyo.

References

Anthes, R.A., Hsie, E.-Y., Kuo, Y.-H., 1987. Description of the Penn State/NCAR Mesoscale Model Version 4 (MM4). National Center for Atmospheric Research, NCAR/TN-282 + STR (PB87 190633/AS), Boulder.

Hiramatsu, N., Hanaki, K., Matsuo, T., 1992. Comparison of energy consumption among seven major cities in Japan. Environmental Systems Research 20, 252–261 (in Japanese with English abstract).

Ichinose, T., Hanaki, K., Matsuo, T., 1993. International comparison of energy consumption in urban area. Proceedings of Environmental Engineering Research 30, 371–381 (in Japanese with English abstract).

Ichinose, T., Hanaki, K., Matsuo, T., 1994. Analyses on geographical distribution of urban anthropogenic heat based on very precise geographical information. Proceedings of Environmental Engineering Research 31, 263–273 (in Japanese with English abstract).

Kessler, R.C., Douglas, S.G., 1992. User's guide to the Systems Applications International Mesoscale Model (Version 2.0). Systems Applications International, SYSAPP-92-085, California.

Kimura, F., Takahashi, S., 1991. The effects of land-use and anthropogenic heating on the surface temperature in the Tokyo metropolitan area: a numerical experiment. Atmospheric Environment 25B, 155–164.

Kondo, H., 1990. A numerical experiment of the "extended sea breeze" over the Kanto Plain. Journal of Meteorological Society of Japan 68, 419–434.

Morita, M., 1993. Study on heat exhaust structure of major cities in Japan. Environmental Systems Research 21, 19–26 (in Japanese with English abstract).

Narita, K., Maekawa, T., 1991. Energy recycling system for urban waste heat. Energy and Buildings 16 (1/2), 553–560.

Pielke, R.A., 1974. A three dimensional numerical model of the sea breezes over South Florida. Monthly Weather Review 102, 115–134.

Saitoh, T., Shimada, T., Hisada, T., 1992. Urban warming and energy consumption in Tokyo metro area. Proceedings of the Intersociety Energy Conversion Engineering Conference 5, 341–348.

Stanhill, G., Kalma, J.D., 1995. Solar dimming and urban heating at Hong Kong. International Journal of Climatology 15, 933–941.

Stull, R.B., 1994. An Introduction to Boundary Layer Meteorology. Kluwer Academic Publishers, Dordrecht.

Therry, G., Lacarrere, P., 1983. Improving the eddy kinetic energy model for planetary boundary layer description. Boundary Layer Meteorology 25, 68–88.

Ulrickson, B.L., Mass, C.F., 1990. Numerical investigation of mesoscale circulations over the Los Angels basin. Part 1, A verification study. Monthly Weather Review 118, 2138–2161.